KINEMATIC TIME DEMIGRATION: THE IMPLICIT CRS APPROACH

M. Glöckner, Y. Yang, C. Vanelle, and D. Gajewski

email: *martina.gloeckner@uni-hamburg.de*

keywords: *time demigration, time migration, i-CRS, velocity, data enhancement*

ABSTRACT

To obtain a subsurface images of the earth seismic time imaging can be applied as a first step. The implicit common reflection surface (CRS) approach provides a powerful tool for time imaging. We can perform a series of processes, e.g. stacking, time migration and demigration. Demigration describes the process of an inverse migration or a back transformation, respectively. A short outline of the time imaging operators is given. Furthermore, the stacking attributes serve as input for a data-driven time migration velocity model building. This means, no user interaction is required to carry out the migration and the following demigration. The demigration is applied to a simple synthetic example to verify general applicability and how noise and the used velocity model influence the demigration. The application to field data illustrates present issues regarding the velocities but nevertheless the possibility to use the demigration as a tool for prestack data enhancement. In addition, it is shown that the demigration operator can be used for rapid forward modelling of simple synthetic prestack data. Ongoing research is related to improving the input data for the demigration to achieve enhanced results.

INTRODUCTION

Huygens's principle (1678) explains the propagation of waves and builds the basis of our comprehension of waves travelling through the earth. First applications to geophysics were introduced by Hagedoorn (1954) with his so-called 'string construction' or 'ruler and compass' method. He describes a migration technique which incorporates parts of Huygens's principle. Claerbout et al. (1996) present two complementary imaging techniques. On the one hand, it is the semicircle superposition which represents a spreading and on the other hand, there is the hyperbola summation method which stands for stacking. These techniques can also be considered as migration (hyperbola summation) and demigration (semicircle superposition). Migration focuses events and correct dips, whereas demigration inverts that process and restores prestack data used for migration. An imaging theory including migration and demigration is presented by Hubral et al. (1996). Huygens's surfaces and isochrons are used as most basic concepts and are combined with dynamic methods to preserve amplitudes. While the main focus in this paper is on depth imaging, Iversen et al. (2012) present a time-based approach. They use reflection times, curvatures, and slopes as parameters to perform the migration and demigration. Furthermore, the demigration can be used for modelling as presented by Whitcombe (1994) and Santos et al. (2000)

In this study, we present a fully data-driven time migration and demigration approach. A possible application of the described imaging techniques is to utilise symmetries and the robustness of time migrated domain, demigrate the image and obtain improved data in the original domain, e.g. for data regularisation and enhancement. In general, all migration techniques have to consider a velocity model. An advantage of our method is that we do not have to estimate or pick the time velocity model because it is automatically derived within the migration algorithm (Bobsin, 2014). The difference to the partial

time demigration introduced by Yang et al. (2015) is reflected in the operator itself and the input data domain. They stay in the migrated prestack domain, whereas we consider zero-offset (ZO) domain as well. Concluding this work, we present first applications of the proposed algorithm to synthetic and field data and discuss the results.

THEORY

This section presents the fundamental theory we need for introducing the time demigration. It contains time imaging operators based on the implicit CRS method. The multiparameter stack is necessary to obtain the CRS attributes. This is an automatic procedure and user interaction is minimised.

Migration operator and velocity

The time migration is designed as a diffraction summation operator, accordingly the implicit CRS prestack time migration (PreSTM) operator in apex coordinates reads:

$$t = \sqrt{\frac{t_{apex}^2}{4} + \frac{(\Delta x_a - h)^2}{V^2}} + \sqrt{\frac{t_{apex}^2}{4} + \frac{(\Delta x_a + h)^2}{V^2}}, \tag{1}$$

where $\Delta x_a = x_m - x_{apex}$ is the midpoint displacement, h is the half-offset, V denotes the time migration velocity and t_{apex} is the apex travel time (Bobsin, 2014). The double-square-root (DSR) operator is similar to a Kirchhoff time migration operator (Yilmaz, 2001).

Schwarz et al. (2014) relate the implicit CRS parameters to the kinematic wave field attributes or CRS parameters, of which the incidence angle α and the radius of curvature of the so-called normal incidence point (NIP) wave, R_{NIP} (Hubral, 1983) are pertinent to this work. They find for the velocity:

$$V = \frac{v_{NMO}}{\sqrt{1 + \frac{v_{NMO}^2}{v_0^2} \sin^2 \alpha}} \quad \text{with} \quad v_{NMO} = \sqrt{\frac{2 v_0 R_{NIP}}{t_{apex} \cos^2 \alpha}}. \tag{2}$$

Equation 2 includes the normal move out (NMO) velocity , v_{NMO}. Furthermore, by considering the incidence angle, we obtain a dip correction. This means, we receive root-mean-square (RMS) like velocities which make them directly applicable for time migration. In our case the velocity (Equation 2) depends on four parameters: α, R_{NIP}, a prescribed near-surface velocity v_0, and the considered time t_{apex}. The kinematic wave field attributes are available after the i-CRS stack. Therefore, the calculation of the migration velocity is a purely data-driven process without user interaction in terms of manual picking.

Demigration operator and workflow

For the inverse process, we change the dependency of Equation 1. In Equation 1, the travel time t is a function of apex time t_{apex} and apex location Δx_a. To obtain the demigration expression, we solve Equation 1 for t_{apex}:

$$t_{apex} = \sqrt{t^2 - \frac{4(\Delta x_a^2 + h^2)}{V^2} + \frac{16 \Delta x_a^2 h^2}{t^2 V^4}}. \tag{3}$$

This is a single-square-root (SSR) expression in contrast to the double-square-root migration operator. The demigration as well as the migration equation are also valid for the post-stack case, where the half offset h vanishes and the equations simplify.

To perform all time imaging processes we stack the data first and simultaneously obtain the desired attributes α and R_{NIP}. As a second step, we run the time migration and calculate the time migration velocity for every sample. The output is a migrated ZO section. As a last step, we use the migrated section to perform the demigration to obtain prestack data in the CMP domain.

In the next section, we investigate possible applications and characteristics of the demigration expression in correspondence with the migration counterpart.

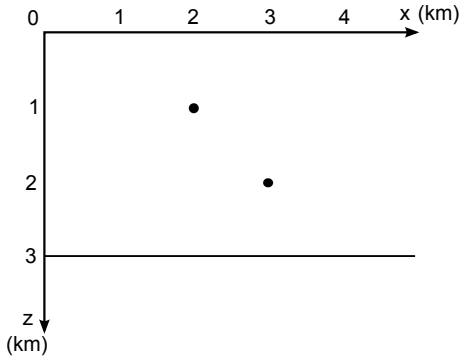

Figure 1: Simple model of two diffractors and a single reflector embedded in a homogeneous constant velocity background medium.

APPLICATIONS

This section presents an overview about the current state of possible applications. Starting with time modelling, we further present a test series using parameters of different qualities as input. In addition, the application to field data is shown.

Forward-modelling by demigration

Simple and fast modelling is an advantage for the investigation of new topics. Often new approaches have special needs and models have to be adjusted. Our demigration operator has some promising properties to perform a fast time modelling. We present a straight forward way to obtain prestack data for further applications.

The idea for the forward modelling is to create a time data set with spikes, which represents the reflections and diffractions. Afterwards, this data set is convolved with a wavelet to obtain a migrated zero-offset section. Then the demigration is applied and provides the prestack data in an extremely fast way. Further ideas to generate more realistic modelled data are as follows:

- to account for geometrical spreading,
- to add an uncertainty to the velocity field, and
- to use a realistic source wavelet, e.g., a minimum phase wavelet.

Some first simple modelling results are presented in the next section.

Tests for the demigration algorithm

In this first generic example we consider a homogeneous model with two diffractors and a single reflector (see Figure 1) to apply the demigration to verify whether it performs correctly or not. Furthermore, we investigate the influence of noise and the sensitivity to the velocity model on the demigrated image. Two sets of migrated ZO sections (see Figure 2) and two different velocity sections (see Figure 3) serve as input, i.e., we perform the demigration for each migrated ZO section for both velocity models leading to four different demigrated prestack data sets.

Figure 2 shows on the left the modelled section as described earlier. A Ricker wavelet with a peak frequency of 30 Hz is used. On the right, we show the processed PreSTM section where noise is added (signal-to-noise ratio is five). The data set is obtained with the SUSYNLV routine where a Ricker wavelet with a peak frequency of 30 Hz is used. Afterwards, it is migrated with the time migration velocity obtained from the stacking attributes. Please note, that the reflection of the modelled section do not have the same width in comparison to the processed PreSTM result. In this case, it is only possible to investigate

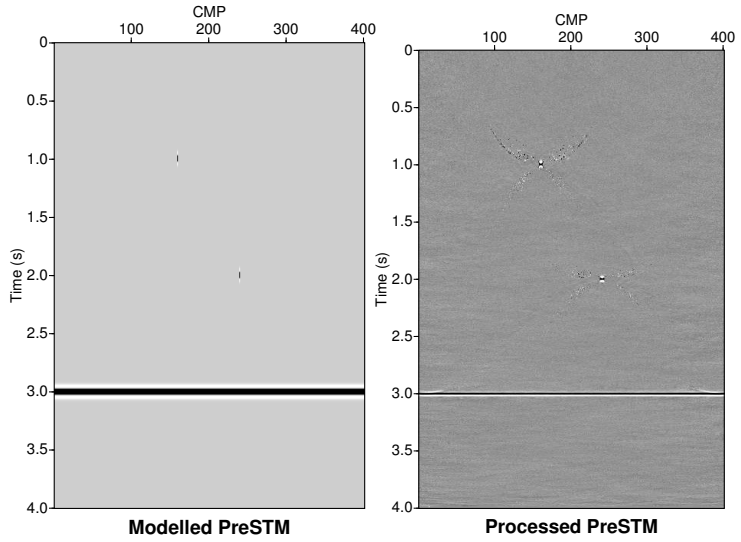

Figure 2: Migrated ZO input sections.

data with the same frequency or the same width of the reflection for different frequencies because different input data sets are generated. The modelled section shows a perfect migrated result for the diffractions which is located on a single trace. Whereas, the processed PreSTM focuses the diffractions over more traces and displays the typical cross-shape artefacts around the object which is related to the limited migration aperture (Hertweck et al., 2003).

To investigate the characteristics of the demigration algorithm we need a time migration velocity model which is shown in Figure 3. The velocities of the diffractions and the reflection are correctly determined and show a certain variations in areas where no events are detected. In addition, we perform the demigration with the constant medium velocity of 2000 m/s. This allows to verify the influence of the velocity model on the demigration.

Figure 4 shows common midpoint (CMP) gathers of the demigrated data. The CMP position is chosen from the middle of the section and with number 200 (see Figure 2). According to Hubral et al. (1996), we choose the same apertures and velocity models for migration and demigration. The midpoint aperture ranges from 500 m at the top to 2000 m at the bottom. The offset aperture starts with zero at zero time and increases to 2000 m which coincides with the maximum offset of the prestack data. We achieve the best and from theory expected demigrated image (Figure 4(a)) under perfect synthetic conditions, i.e., for a correct velocity model and a migrated ZO section without migration artefacts serves as input for demigration. Further observations in columns and rows are visible. The images of the first row (Figure 4(a) and 4(b)) show, that a constant medium velocity model leads to continuous events, whereas the determined velocity in the second row (Figure 4(c) and 4(d)) leads to disrupted or non-continuous events at larger offsets. This is due to the fact that the migration velocity is calculated from zero-offset attributes and therefore not suitable for large offsets. Using noisy data, as in the second column (Figure 4(b) and 4(d)), we observe weak periodic patterns displaying the move out of the original evens. Noise is visible in the upper part of each image due to boundary effects.

Figure 5 shows common offset ($h = 1000$ m) sections of the demigrated pre-stack data. In general, the same conclusions as for Figure 4 hold. An incorrect velocity model perturbs events, but in contrast to the previous figure, noise does not lead to periodic events along the midpoint direction for a single particular offset. The Figures 5(c) and 5(d) show discontinuous events in a CO section due to the influence of the determined velocity model . Figures 5(a) and 5(b) show typical aperture artefacts at the beginning and at the end of the reflection. Furthermore, it would be preferable to obtain larger diffraction

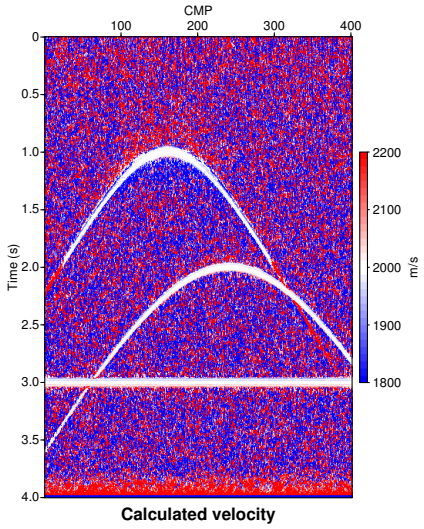

Figure 3: Time migration velocity model computed from stacking parameters. The homogeneous medium velocity is 2000 m/s. The events are detected with a reliable velocity model which is close to the medium velocity.

tails but this is probably an aperture issue and can be investigated or resolved in ongoing work. Again, we observe noise in the upper parts of the images.

This test series shows that the demigration operator performs well for synthetic conditions. Additionally we have to consider two observations. First, an incorrect velocity model results in disrupted events. Second, noise produces weak periodic patterns. In the outlook we suggest a strategy to resolve these problems.

Field data example

TGS provided a marine data set from the Eastern Mediterranean. The acquired seismic line is located in the Levantine basin, which is bounded by the Cyprus arc in the north, the Levantine coast in the east and the Egyptian coast in the south. Complex salt tectonics are characteristic features of this basin.

Figure 6 shows the determined time migration velocity model used for migration and demigration. We applied a global optimisation routine to obtain smoother stacking attributes for the determination of the velocities. We can see layering of sediments indicated by slow increasing velocities, e.g. on the right side. The first ocean bottom multiple is partly removed but still there are influences which lead to smaller velocities at later times indicated in blue colours on the left. Diffraction hyperbolas are visible in the image. In this work, we focus on the demigration of the field data. Migrated images are shown by Bobsin (2014). Comparisons are made between the demigrated data and the raw data. According to Hubral et al. (1996), we choose the same apertures and velocity models for migration and demigration. We used the same apertures for migration and demigration with the exception that the minimum offset of the demigration is zero due to implementation reasons. The midpoint aperture ranges from 1500 m to 2500 m and the offset aperture from 1000 m to 7000 m.

Figure 7 shows CMP gathers of the original (left) and demigrated (middle) data as well as the corresponding time migration velocities (right) at CMP position 1100 (see Figure 6). We see that the events in the demigrated image are disrupted and discontinuous, especially for larger offsets. The reason for this is the already smoothed velocity function, which contains noise and spikes. Larger deviations arise

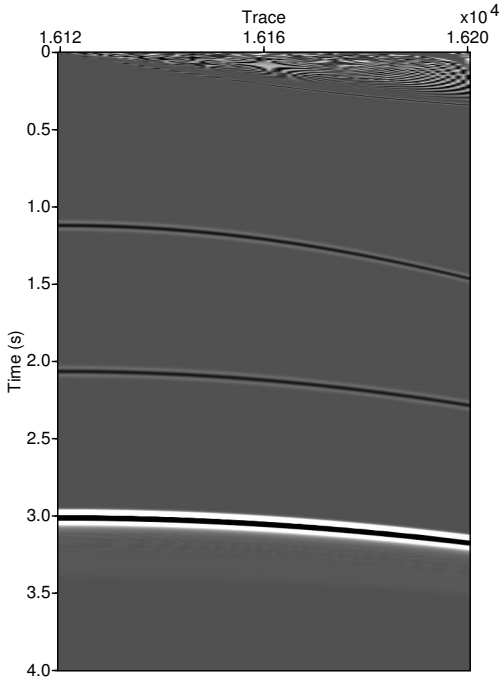

(a) Modelled data with constant velocity.

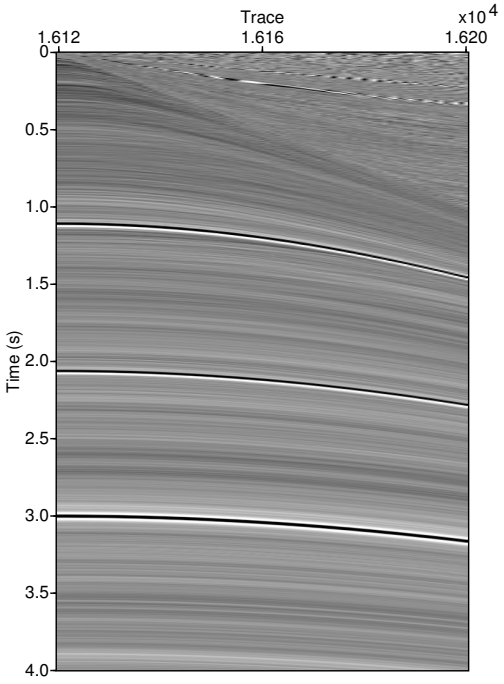

(b) Processed data with constant velocity.

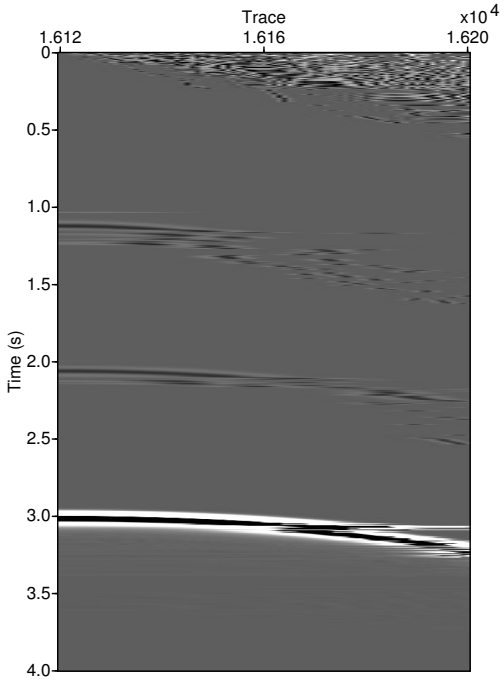

(c) Modelled data with determined velocity.

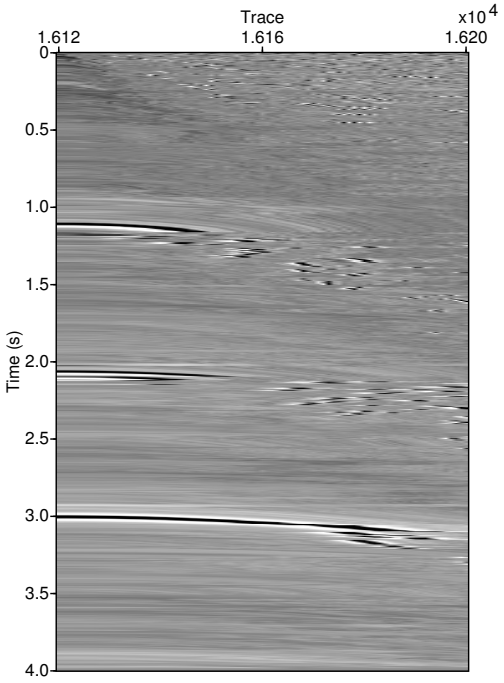

(d) Processed data with determined velocity

Figure 4: CMP gather of different demigrated images. The first two events belong to the diffractions and the event starting at 3 s denotes the reflection.

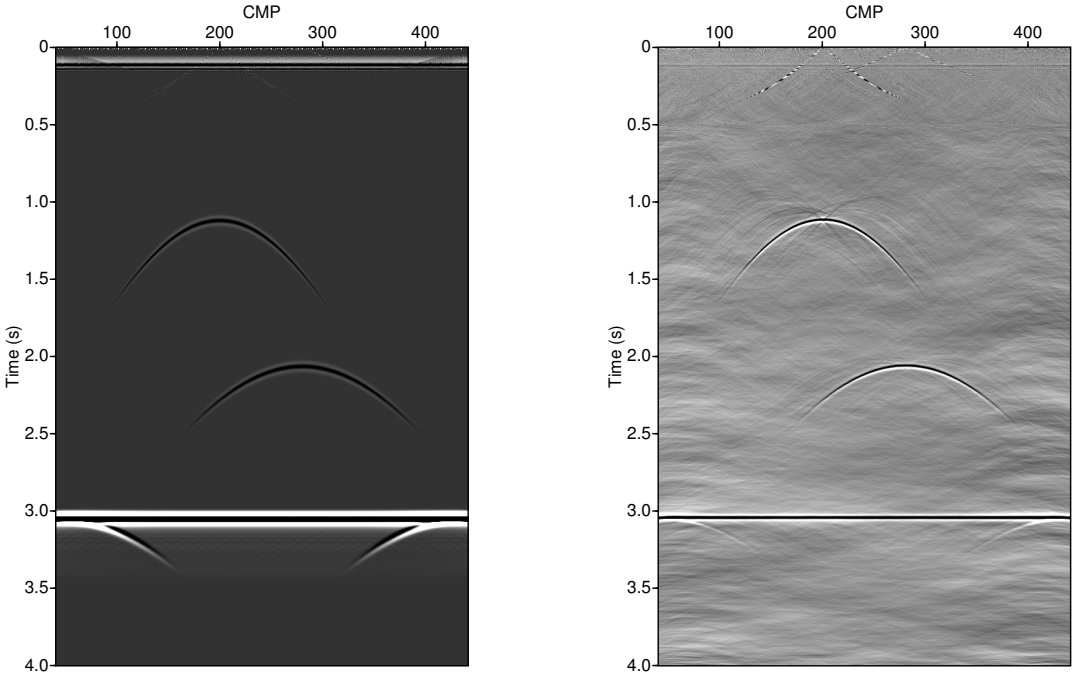

(a) Modelled data with constant velocity.

(b) Processed data with constant velocity.

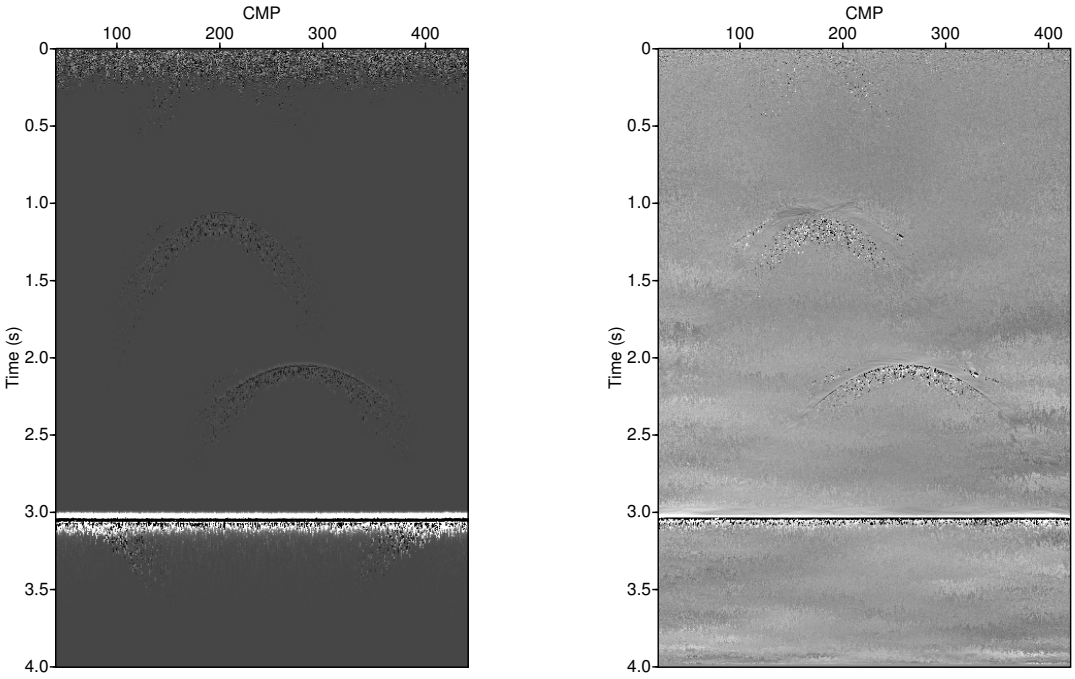

(c) Modelled data with determined velocity.

(d) Processed data with determined velocity

Figure 5: Common offset section ($h = 1000$ m) of different demigrated images. The two hyperbolas are the diffractions and the planar line is the reflection.

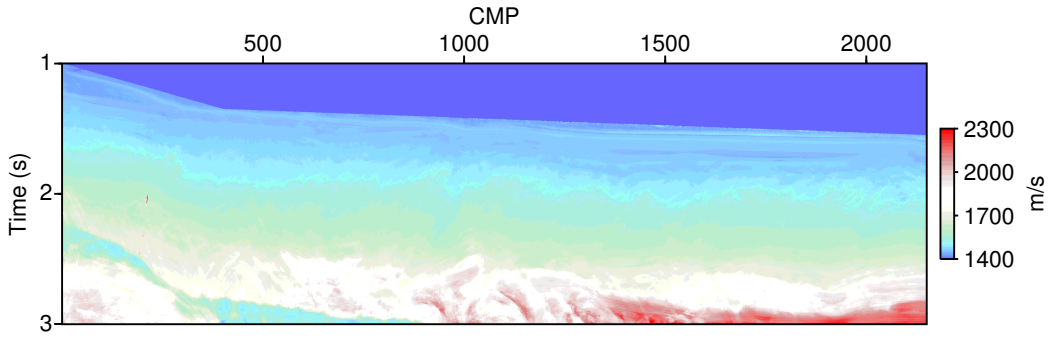

Figure 6: Determined time migration velocities for the field data. The water column is muted and only a small part above the seafloor is visible. Boundary effects lead to the high velocities at the edges. The color scale is clipped.

for increasing time. We conclude that the demigration algorithm is more influenced by an incorrect velocity model than the migration. This observation calls for an improvement of the velocity model and is considered in the outlook. Furthermore, the individual events are stretched in comparison with the original data. Again, we see noise in the upper part of the demigrated image. Nevertheless, the demigration recovers the most prominent events but the resolution is decreased.

Figure 8 shows an common offset section with $h = 500$ m for the original data on top and the demigrated on the bottom. The demigration stretches the events and decreases the resolution. On the other hand, we are able to reconstruct the data with an automatic generated time velocity model without further enhancement, e.g. migration velocity analysis (MVA). In contrast to the previous Figure 7, the events are continuously imaged in the common offset section.

CONCLUSIONS AND OUTLOOK

We presented a time migration and demigration method, which incorporates automatic time velocity model building. The operator for the forward and backward transformation between different domains is based on the implicit CRS approach. We presented a workflow to use the demigration operator for forward modelling of simple synthetic data sets. . We presented an application for an idealized input data set to investigate the feasibility of the demigration. As a result, we see that the demigration operator performs well under perfect synthetic conditions, while noise and velocity errors degrade the result. This observation was confirmed by the application to field data. In conclusion, a good velocity model is required to obtain reliable demigrated prestack data.

The observed differences in the migration-demigration processing chain are an expression of an imperfect operator. These differences are be related to errors in the operator. If these errors may be quantified these results could help to identify illumination and velocity issues to improve the image the migrated domain. This will be a subject of future work.

Ongoing and other future work therefore, also includes improvements in the automatic determination of migration velocities analysis to obtain a better time migration velocity model and prestack time migrated images which will lead to improved input data for the demigration. As a first approach, we want to use the coherence to weight the velocity model and interpolate areas where the migrated coherence shows insufficient results. Smoothing of the velocity model can also be applied as an additional option. Furthermore, the application as a partial migration and demigration operator is also possible. The prestack

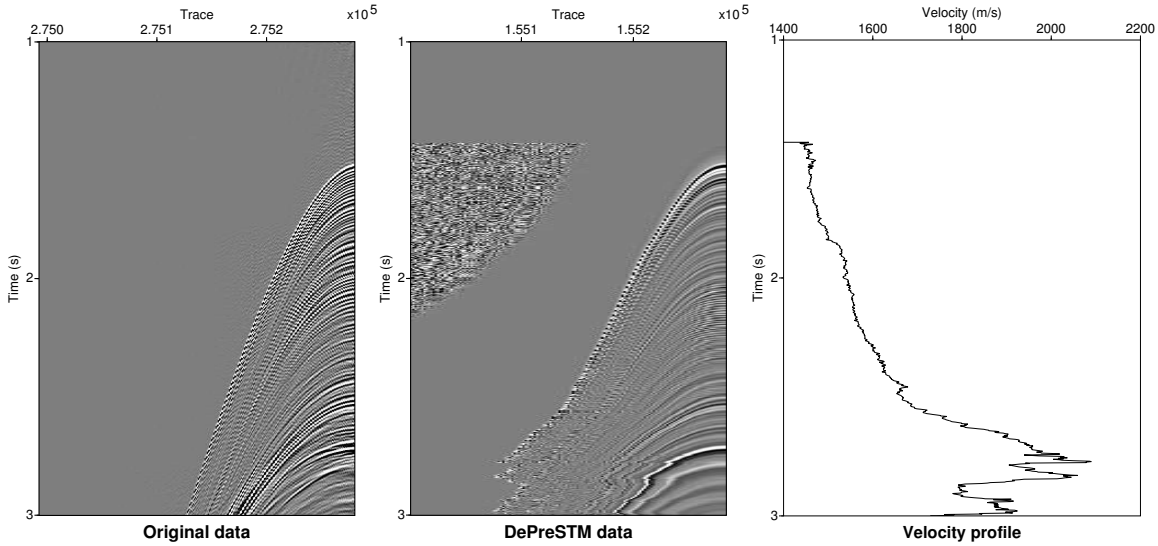

Figure 7: Comparison of CMP gathers and corresponding time migration velocity profile for the TGS data set.

data quality would be enhanced (see also Yang et al. (2015)). The partial migrated domain promises to be less error-prone because migration is only performed in the midpoint direction.

ACKNOWLEDGEMENTS

We thank the members of the Applied Seismic Group Hamburg for continuous discussions, especially Jan Walda for providing the global attributes and Sophia Wissmath and Benjamin Schwarz for proofreading. This work was kindly supported by the sponsors of the Wave Inversion Technology (WIT) Consortium.

REFERENCES

Bobsin, M. (2014). Time Migration applying the i-CRS Operator. Master's thesis, University Hamburg.

Claerbout, J., Green, C., and Green, I. (1996). *Imaging the Earth's Interior*. Free Software Foundation.

Hagedoorn, J. (1954). A process of seismic reflection interpretation. *Geophysical Prospecting*, 2:85–127.

Hertweck, T., Jäger, C., Goertz, A., and Schleicher, J. (2003). Aperture effects in 2.5D Kirchhoff migration: A geometrical explanation. *Geophysics*, 68:1673–1684.

Hubral, P., Schleicher, J., and Tygel, M. (1996). A unified approach to 3-D seismic reflection imaging, Part I: Basic concepts. *Geophysics*, 61(3):742–758.

Iversen, E., Tygel, M., Ursin, B., and de Hoop, M. (2012). Kinematic time migration and demigration of reflections in pre-stack seismic data. *Geophysical Journal International*, 189:1635–1666.

Santos, L., Schleicher, J., Tygel, M., and Hubral, P. (2000). Seismic modeling by demigration. *Geophysics*, 65(4):1281–1289.

Schwarz, B., Vanelle, C., Gajewski, D., and Kashtan, B. (2014). Curvatures and inhomogeneities: An improved common-reflection-surface approach. *Geophysics*, 79(5):S231–S240.

Whitcombe, D. (1994). Fast model building using demigration and single-step ray migration. *Geophysics*, 59(3):439–449.

Yang, Y., Vanelle, C., Glöckner, M., and Gajewski, D. (2015). Kinematic time demigration: the CSP approach. *Annual WIT Report*, 19:136–148.

Yilmaz, O. (2001). *Seismic Data Analysis*. SEG, Tulsa.

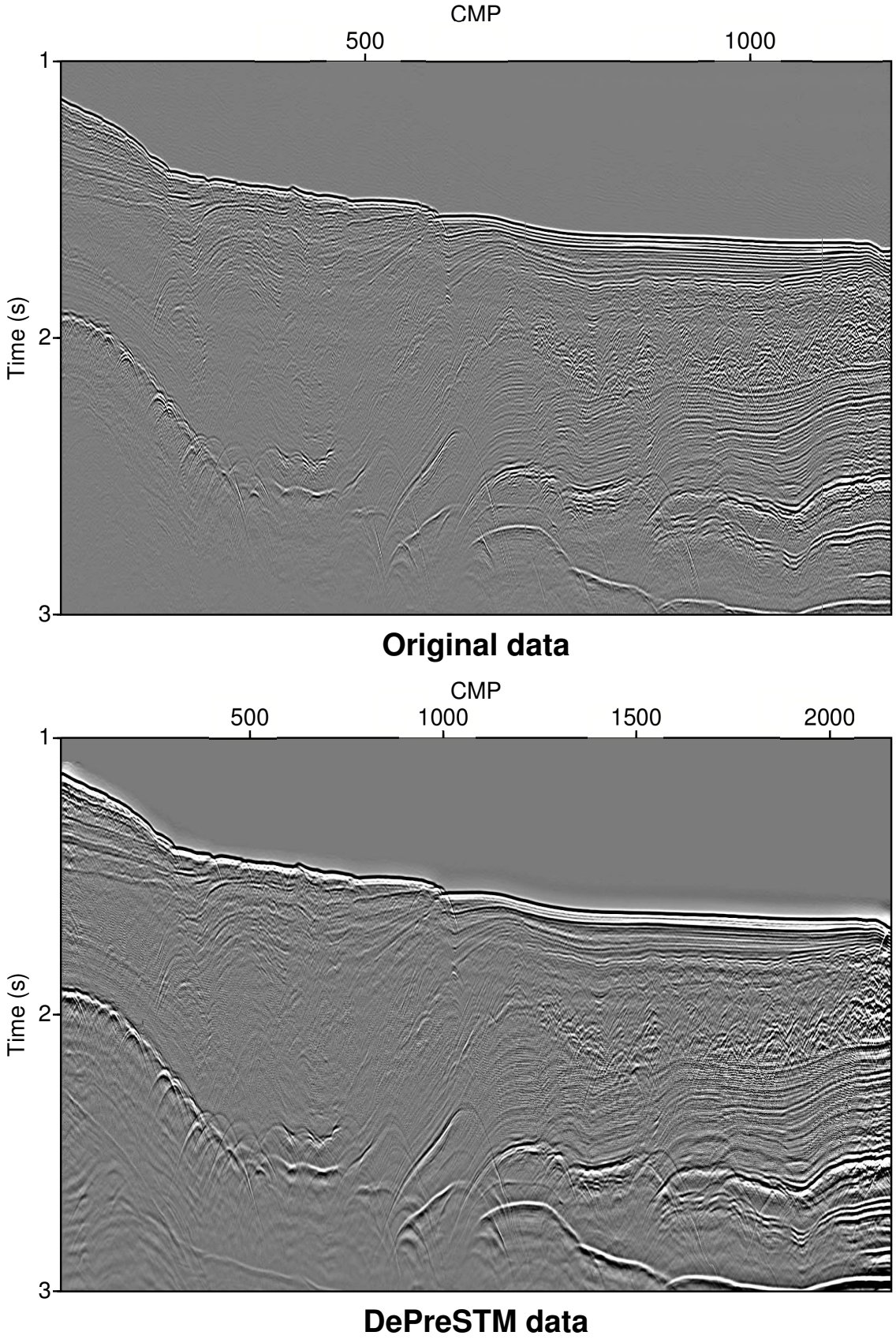

Figure 8: Common offset section $h = 500$ m for original (top) and demigrated (bottom) data. Major events are well recovered by the demigration.